DEVELOPMENTAL BIOLOGY

The pro-apoptotic function of the *C. elegans* BCL-2 homolog CED-9 requires interaction with the APAF-1 homolog CED-4

Nolan Tucker[1], Peter Reddien[1]†, Bradley Hersh[1]‡, Dongyeop Lee[1], Mona H. X. Liu[1,2], H. Robert Horvitz[1]*

In *Caenorhabditis elegans*, apoptosis is inhibited by the BCL-2 homolog CED-9. Although canonically anti-apoptotic, CED-9 has a poorly understood pro-apoptotic function. CED-9 is thought to inhibit apoptosis by binding to and inhibiting the pro-apoptotic *C. elegans* APAF-1 homolog CED-4. We show that CED-9 or CED-4 mutations located in their CED-9–CED-4 binding regions reduce apoptosis without affecting the CED-9 anti-apoptotic function. These mutant CED-9 and CED-4 proteins are defective in a CED-9–CED-4 interaction in vitro and in vivo, revealing that the known CED-9–CED-4 interaction is required for the pro-apoptotic but not for the anti-apoptotic function of CED-9. The pro-apoptotic CED-9–CED-4 interaction occurs at mitochondria. In mammals, BCL-2 family members can activate APAF-1 via cytochrome c release from mitochondria. The conserved role of mitochondria in CED-9/BCL-2–dependent CED-4/APAF-1 activation is notable and suggests that understanding how CED-9 promotes apoptosis in *C. elegans* could inform the understanding of mammalian apoptosis and how disruptions of apoptosis promote certain human disorders.

INTRODUCTION

Programmed cell death is an evolutionarily conserved process essential for proper development and tissue homeostasis in metazoans (*1*, *2*). In humans, either excessive or insufficient cell death can result in diseases, including cancers and certain autoimmune and neurodegenerative disorders (*3*–*5*). In *Caenorhabditis elegans*, four genes—*egl-1*, *ced-9*, *ced-4*, and *ced-3*—are primarily responsible for the control of apoptotic cell death (*6*–*8*). It has been proposed based on genetic, protein interaction, and localization studies that CED-9 (a homolog of mammalian BCL-2) protects cells from apoptosis by sequestering the pro-apoptotic protein CED-4 (APAF-1 in mammals) to mitochondria (*9*–*11*). According to this model, in cells fated to die, EGL-1 (a BH3-only member of the Bcl-2 superfamily) binds CED-9, causing a conformational change in CED-9 that results in the release of CED-4 (*12*). After its release from CED-9, CED-4 localizes to the perinuclear membrane where it activates the caspase CED-3 (*10*, *11*). A strong *ced-9* loss-of-function mutation leads to maternal-effect lethality, presumably as a consequence of excessive cell death, and animals carrying loss-of-function mutations in both *ced-9* and a downstream cell-death promoting gene—either *ced-4* or *ced-3*—are viable because cell death is prevented. However, and counterintuitively, a loss-of-function mutation in *ced-9* can enhance the partial cell-death defect of animals with a weak loss-of-function mutation in the pro-apoptotic caspase gene *ced-3* (*13*). This finding suggests that, in addition to its anti-apoptotic role, CED-9 has a pro-apoptotic function.

The existence of a pro-apoptotic function of CED-9 implies that the canonical model for *C. elegans* cell death, in which CED-9 functions only as an anti-apoptotic protein, is incomplete. Furthermore, the canonical model proposes that, in living cells, cell death is blocked by the CED-9–dependent sequestration of CED-4 to mitochondria. However, in *ced-9(n1653ts)* temperature-sensitive mutant animals at a permissive temperature, some CED-4 protein is localized to the perinuclear membrane, as assayed by anti–CED-4 polyclonal antibody localization (*9*). The *ced-9(n1653ts)* allele, causes lethality at nonpermissive temperatures [like *ced-9(0)* alleles] but at permissive temperatures allows viability [like *ced-9(+)* and weak *ced-9(lf)* loss-of function alleles]. The observation that CED-4 protein can be localized to the perinuclear membrane without causing lethality suggests that CED-4 localization at the perinuclear membrane is not sufficient to drive apoptosis. In addition, despite the ability of *ced-9(lf)* alleles to enhance ectopic cell survival caused by weak loss-of-function alleles in the cell-death promoting *ced-3* gene, loss of *ced-9* function in the presence of a weak *ced-3* loss-of-function mutation results in CED-4 localization to the perinuclear membrane (*9*). Furthermore, overexpression of a functional CED-4::GFP (green fluorescent protein) transgene fails to induce the death of germ cells in which the CED-4::GFP protein is localized to the perinuclear membrane (*14*), again uncoupling CED-4 localization at the perinuclear membrane from the activation of apoptotic death. In short, these observations suggest that CED-4 localization at the perinuclear membrane is not sufficient to cause cell death.

Here, we report that mutations in the known CED-9–CED-4 binding region cause a loss of the pro-apoptotic but not the anti-apoptotic function of CED-9. In addition, these mutations prevent the CED-9–dependent sequestration of CED-4 to mitochondria. Our results suggest that—opposite to the canonical model for *C. elegans* cell death in which a CED-9–CED-4 interaction (and consequent CED-4 mitochondrial localization) are anti-apoptotic—a CED-9–CED-4 interaction (and possibly CED-4 mitochondrial localization) are required for the pro-apoptotic function of CED-9. Because *C. elegans* cell-death genes show notable homology to mammalian cell-death genes (*13*–*17*), these findings have implications for

[1]Howard Hughes Medical Institute, Department of Biology, Massachusetts Institute of Technology, Cambridge, MA 02139, USA. [2]Harvard Medical School, Boston, MA 02115, USA.
*Corresponding author. Email: horvitz@mit.edu
†Present address: Whitehead Institute, Department of Biology, Massachusetts Institute of Technology, Cambridge, MA 02139, USA.
‡Present address: Department of Biology, Allegheny College, Meadville, PA 16335, USA.

our understanding of the functions of mammalian BCL-2 family members in cell death and how perturbation of their functions can affect human diseases, including certain neurogenerative disorders and cancers.

RESULTS

CED-9 has a pro-apoptotic function

In the canonical model of *C. elegans* apoptosis, the anti-apoptotic protein CED-9 prevents apoptosis by sequestering the pro-apoptotic CED-4 protein to mitochondria (Fig. 1, A and B). *ced-9(lf)* mutations cause maternal-effect lethality, presumably via excessive apoptosis because mutations in the downstream pro-apoptotic genes *ced-3* and *ced-4* suppress this lethality. However, *ced-9(lf)* mutations can also enhance the cell-death defect caused by a weak loss-of-function mutation in either *ced-3* or *ced-4* (*13*), indicating the existence of a poorly understood pro-apoptotic role for *ced-9*. One such enhancement of a cell-death defect by *ced-9(lf)* mutations involves the ventral cord (VC) neurons in the ventral nervous system. In wild-type (WT) animals, six VC neurons (P3-8.aap) survive and express the GFP reporter *nIs106[P_{lin-11}::GFP]*, whereas six VC homologs (P1-2,9-12.aap) undergo apoptosis (*18*). In mutants carrying a null allele of either *ced-3* or *ced-4*, the six VC homologs that normally die instead survive, differentiate, and express characteristics of the VC neurons (*19*), including expression of the *P_{lin-11}::GFP* reporter; five of these six "undead" VC-like cells can be reliably scored

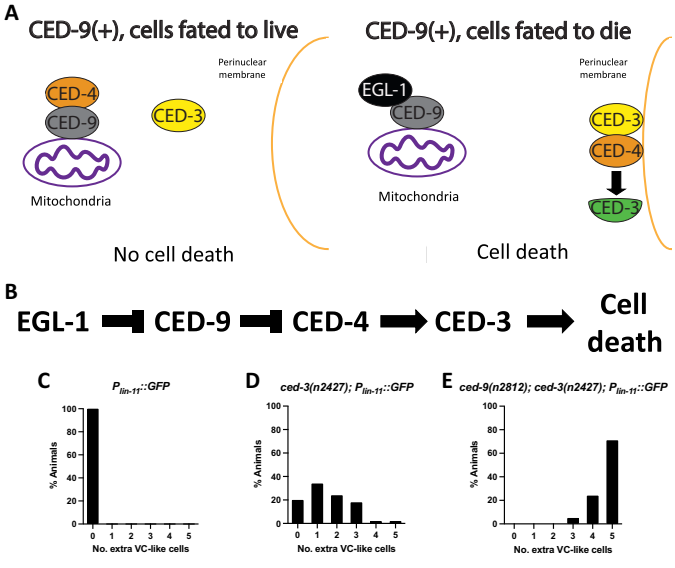

Fig. 1. *ced-9* has a noncanonical pro-apoptotic function. (**A**) Canonical model for apoptosis in *C. elegans*. CED-9 acts to prevent cell death by sequestering the pro-apoptotic protein CED-4 to mitochondria. Cells fated to die express the pro-apoptotic EGL-1, which binds CED-9, causing a conformational change in CED-9 that results in the release of CED-4 from mitochondria. After its release from CED-9, CED-4 localizes to the perinuclear membrane, where it activates the caspase CED-3, thus inducing cell death. (**B**) Canonical genetic pathway for apoptosis in *C. elegans*. (**C** to **E**) Defects in cell killing, as assayed using the transgene *nIs106[P_{lin-11}::GFP]*, a GFP reporter expressed in both the VC motor neurons and "extra" VC-like undead cells. (C) In wild-type animals, this transgene detects no extra VC-like cells ($n = 50$). (D) *ced-3(n2427)* causes the ectopic survival of ~1.7 extra VC-like cells ($n = 50$). (E) The null allele *ced-9(n2812)* enhances the cell-killing defect caused by *ced-3(n2427)* from ~1.7 to ~4.7 extra VC-like cells ($n = 50$).

using this GFP reporter. Whereas *ced-3* null mutants show ectopic survival of about 5 extra cells, animals carrying a weak loss-of-function allele of *ced-3*, *ced-3(n2427)*, show ectopic survival of about 1.7 extra VC-like cells (Fig. 1, C and D) (*20*). By contrast, when *ced-3(n2427)* is paired with the *ced-9* null allele *ced-9(n2812)*, these double-mutant animals show roughly 4.7 extra VC-like cells (Fig. 1E). This result indicates that a lack of *ced-9* function can cause a notable increase in VC cell survival, indicative of the poorly understood pro-apoptotic function of *ced-9*.

An EMS screen for *ced-3(lf)* enhancers generated CED-9–CED-4 binding region mutations

In an earlier work, we described anethyl methanesulfonate (EMS) screen for enhancers of the cell-killing defect caused by *ced-3(n2427)* (Fig. 2A) (*20*). In addition to those mutations previously reported, this screen generated an atypical allele of *ced-9*, *ced-9(n3377)*. Like most *ced-9(lf)* alleles, such as the null allele *ced-9(n2812)*, *ced-9(n3377)* enhanced the cell-killing phenotype caused by *ced-3(n2427)* and did so to an extent similar to that caused by a *ced-9* null allele (Figs. 1E and 2B). By contrast, unlike typical *ced-9(lf)* alleles, which on their own cause maternal-effect recessive lethality because of excessive cell death (*7*), *ced-9(n3377)* when crossed into a *ced-3(+)* background was viable and caused a decrease in cell death: In *ced-3(+); ced-9(n3377)* animals, about 2.6 extra VC-like cells survived, in contrast to 0 extra VC-like cells in *ced-3(+); ced-9(+)* animals (Figs. 1C and 2C). Thus, *ced-9(n3377)* mutants lack the maternal-effect lethal (excess cell death) phenotype characteristic of most loss-of-function alleles of *ced-9*, such as *ced-9(n2812)* (Fig. 2D) and hence retain the anti-apoptotic function of *ced-9*. To preclude background mutations as the cause of this atypical phenotype of *ced-9(n3377)* animals, we used CRISPR to independently generate the *n3377* (E74K) *ced-9* mutation. The recreated allele, *ced-9(n6676)*, resulted in the same phenotype as did *ced-9(n3377)* (Fig. 2E), confirming that *n3377* caused the atypical phenotype.

The cell-death defect of *ced-9(n3377)* animals is recessive: Like *ced-9(+)/ced-9(+)* animals, *n3377*/+ animals had 0 extra VC-like cells (Fig. 2F). This observation indicates that the *ced-9(n3377)* mutation causes a decrease in the pro-apoptotic function of *ced-9* rather than an increase in the cell-death inhibitory function of *ced-9*. We next confirmed that *ced-9(n3377)* results in ectopic VC-like cells by perturbing cell death rather than a process other than cell death. Specifically, *ced-9(n3377)* failed to enhance the ectopic VC-like cell survival phenotype of animals carrying *ced-3(n3692)*, a null allele of *ced-3* that prevents cell death altogether (Fig. 2, G and H). We conclude that *n3377* likely causes a loss of the cell-death promoting function of *ced-9*. In short, because *ced-9(n3377)* animals showed a defect in executing cell death but did not show maternal-effect lethality, *ced-9(n3377)* animals seem to lack the pro-apoptotic but retain the anti-apoptotic function of *ced-9*.

The *ced-9(n3377)* missense mutation E74K is located in a domain of CED-9 thought to be involved in binding CED-4, based on the crystal structure of a CED-9–CED-4 complex (Fig. 2, I and J) (*21*). The location and nature of the E74K mutation indicate that *n3377* likely disrupts CED-4 binding. Given the cell-killing defect of *ced-9(n3377)* mutants, one possibility is that the pro-apoptotic function of *ced-9* depends on an interaction with CED-4. This hypothesis contradicts the canonical model for *C. elegans* apoptosis, according to which a loss of CED-9–CED-4 interaction should cause widespread ectopic apoptosis and maternal-effect lethality.

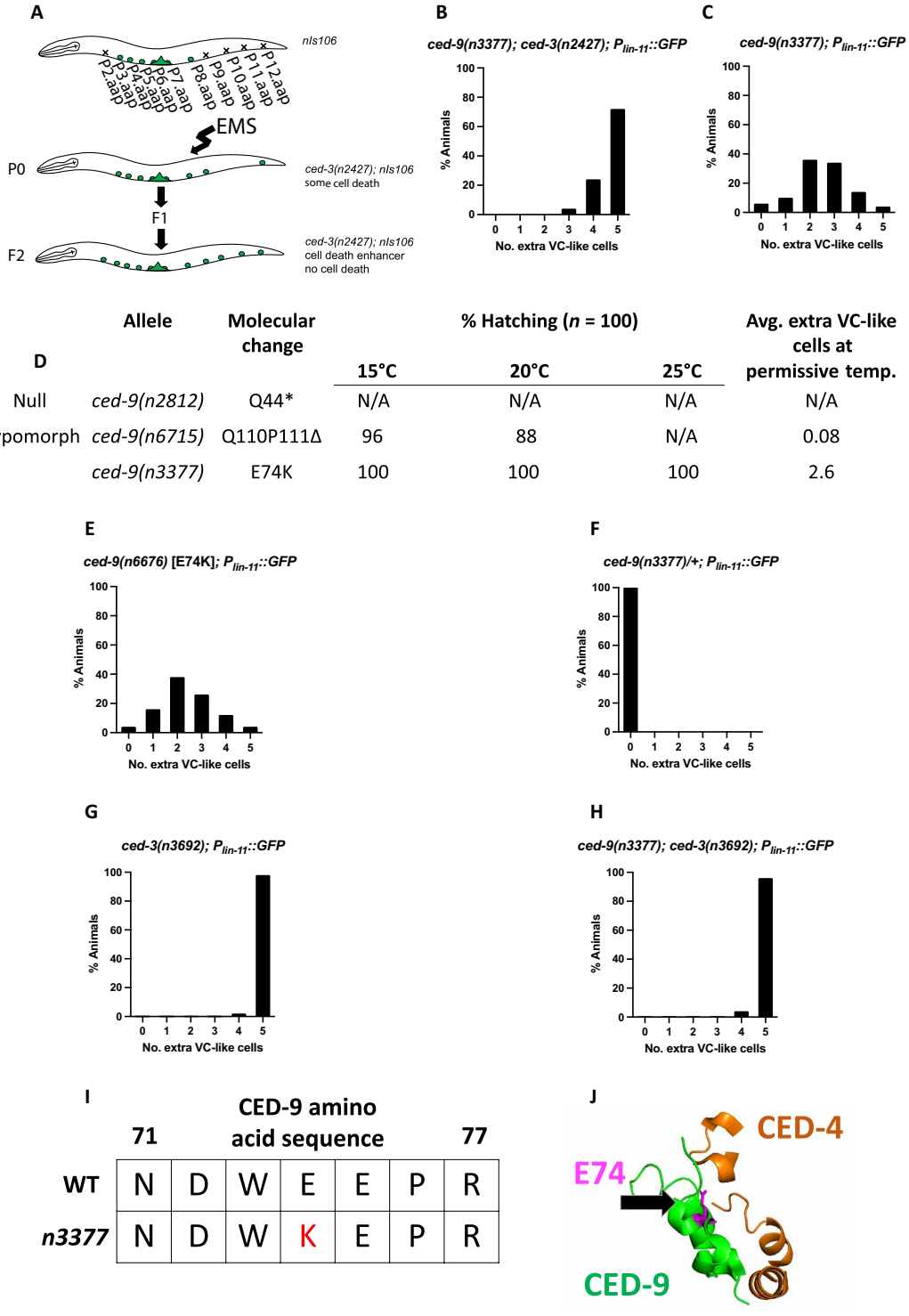

D

	Allele	Molecular change	% Hatching (*n* = 100) 15°C	20°C	25°C	Avg. extra VC-like cells at permissive temp.
Null	*ced-9(n2812)*	Q44*	N/A	N/A	N/A	N/A
Hypomorph	*ced-9(n6715)*	Q110P111Δ	96	88	N/A	0.08
	ced-9(n3377)	E74K	100	100	100	2.6

I

CED-9 amino acid sequence

	71						77
WT	N	D	W	E	E	P	R
n3377	N	D	W	K	E	P	R

Fig. 2. An EMS screen for enhancers of *ced-3(n2427)* isolated a mutation that disrupts the CED-4 binding region of CED-9. (**A**) An EMS screen for enhancers of the cell-death defect mediated by a weak loss-of-function allele of *ced-3*, *ced-3(n2427)* (*20*). (**B** and **C**) This screen identified *ced-9(n3377)*, which is homozygous viable, enhances the cell-killing defect caused by *ced-3(n2427)* and results in the ectopic survival of ~2.6 extra VC-like cells on its own (*n* = 50). (**D**) The *ced-9* null allele, *ced-9(n2812)*, does not produce viable progeny at 15°, 20°, and 25°C. A partial loss-of-function allele of *ced-9*, *ced-9(n6715)*, shows some maternal-effect lethality at 15° and 20°C and fails to produce viable progeny at 25°C; this allele causes the ectopic survival of 0.08 VC-like cells on average at 20°C. A total of 100% of eggs laid by *ced-9(n3377)* hatch at 15°, 20°, and 25°C, and *ced-9(n3377)* animals have ~2.6 ectopically surviving VC-like cells on average at 20°C. N/A, not applicable. (**E**) *n3377* was recreated in a strain free from background mutations caused by EMS to rule out the possibility that background mutations caused by EMS cause the loss of cell-killing phenotype (*n* = 50). (**F**) The cell-killing defect caused by *n3377* is recessive (n = 50). (**G** and **H**) The *ced-3* null allele *n3692* is not enhanced by *ced-9(n3377)*, indicating that *ced-9(n3377)* causes extra VC-like cells by blocking apoptosis (*n* = 50). (**I** and **J**) *ced-9(n3377)* carries a missense mutation (E74K) in the CED-9–CED-4 binding region as defined by crystallographic studies (*21*).

In addition to *ced-9(n3377)*, the screen described above also generated the *ced-4* allele *n3392*, which is an R117S missense mutation. We independently generated this mutation using CRISPR in a strain free from background mutations caused by EMS and named this allele *ced-4(n6703)* (see Methods). This *ced-4* allele was of interest because R117S is located in the presumptive CED-9 binding region of CED-4 (Fig. 3, A and B) and is therefore likely to disrupt a CED-9–CED-4 interaction. *ced-4(n6703)* animals were viable and displayed a weak cell-killing defect: An average of 1.0 extra VC-like cells were present in these animals, as opposed to the 4.9 extra VC-like cells present in *ced-4(n1162)* null mutant animals (Fig. 3, C and D and Table 1). Both *ced-9(n3377)* and *ced-4(n6703)* also had extra M4-like and RIM/RIC-like cells (table S1), indicating that the cell-killing defect is not limited to VC-like cells. *ced-4(n6703)* did not suppress the maternal-effect lethal phenotype caused by the strong loss-of-function allele *ced-9(n1950 n2161)*. In this way, *ced-4(n6703)* is similar to a wild-type *ced-4(+)* allele and unlike a *ced-4(0)* null allele, e.g., *n1162* (Table 1). These observations are consistent with the hypothesis that *n6703* causes a partial loss of *ced-4* function. However, (i) *ced-4(n6703)* mutants displayed a greater cell-killing defect (1.0 extra VC-like cells) than did two distinct weak hypomorphic reduction-of-function *ced-4* mutants, *ced-4(n2879)* and *ced-4(n2860)* (0.02 and 0.44 extra VC-like cells, respectively); and (ii) *ced-4(n6703)* failed to rescue the maternal-effect lethality of *ced-9(n1950 n2161)*, whereas both of the apparently weaker alleles, *ced-4(n2879)* and *ced-4(n2860)*, did so (Table 1). These observations indicate that *ced-4(n6703)* does not cause a slight general reduction in *ced-4* function but rather—just like *ced-9(n3377)*—specifically results in extra VC-like cells while not affecting the maternal-effect lethal phenotype that is caused by a loss of the anti-apoptotic function of *ced-9*. Because *ced-9(n3377)* mutants are likely deficient in their ability to form a CED-9–CED-4 interaction and lack the pro-apoptotic but not the anti-apoptotic function of *ced-9*, we propose that *ced-4(n6703)* mutants lack a function of *ced-4* needed for the pro-apoptotic function of *ced-9*. In short, these observations suggest that *ced-4(n6703)* causes a cell-killing defect because of a lack of a CED-4(R117S) interaction with CED-9 and that CED-4(R117S) is otherwise functional. These results further suggest that perturbing a CED-9–CED-4 interaction by altering a CED-9–CED-4 interaction domain in either CED-9 or CED-4 is sufficient to cause a cell-killing defect.

Additional mutations in the CED-4 binding region of CED-9 cause a cell-killing defect

Our observations concerning *ced-9(n3377)* raise the possibility that other *ced-9* mutations affecting a CED-9–CED-4 interaction also

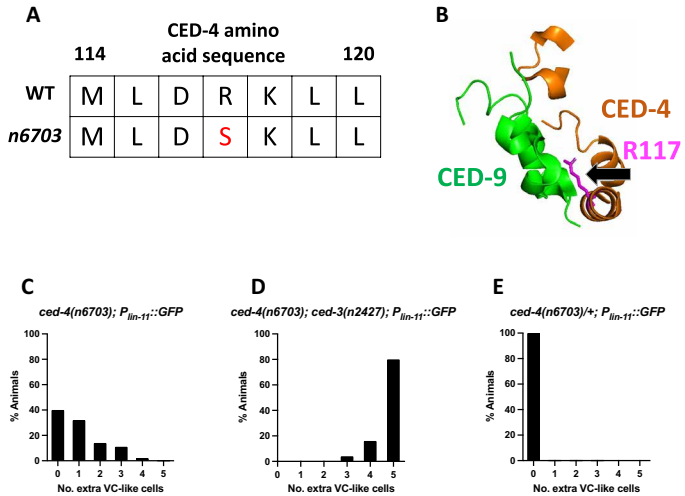

Fig. 3. *ced-4(n6703)* causes ectopic VC-like cell survival and contains a mutation in the CED-9 binding region. (**A** and **B**) CED-4[R117S] is a missense mutation in the CED-9 binding region of CED-4, as defined by crystallographic studies (*21*). (**C** to **E**) *ced-4(n6703)* enhances the cell-killing defect caused by *ced-3(n2427)* and results in a recessive cell-death defect that causes ~1.0 extra VC-like cells on its own ($n = 50$).

Table 1. *ced-4(n6703)* does not result in a simple reduction in *ced-4* function. *ced-4(n6703)* causes a stronger cell-killing defect than do *ced-4(n2860)* and *ced-4(n2879)*, as shown by VC-like cell survival. However, *ced-4(n2879)* and *ced-4(n2860)* but not *ced-4(n6703)* can rescue the maternal-effect lethality caused by the *ced-9* loss-of-function allele *ced-9(n1950 n2161)* ($n = 50$). The mutation *unc-69(e587)* is present in the background of all listed *ced-4 ced-9(n1950 n2161)* double mutants because this marker is closely linked to *ced-9* and was used to follow *ced-9(n1950 n2161)* during crossing.

ced-4 allele	Molecular change	Avg. extra VC-like cells (P_{lin-11}::*GFP*)	Rescues *ced-9(n1950 n2161)*
Wild-type	–	0	No
n2879	E276K	0.02	Yes
n2860	E263K	0.44	Yes
n6703	R117S	1.0	No
n3141	R53K	3.4	Yes
n1162 (null)	Q80Ochre	4.9	Yes

specifically disrupt the cell-killing function of *ced-9*. To test this possibility, we used CRISPR to generate additional mutations in the known CED-4 binding region of CED-9 (*21*). We performed these experiments using *ced-3(+)* animals carrying the transgene *nIs106* and screened for worms that that were both viable and showed ectopic VC-like cell survival. This approach generated five alleles of *ced-9*; each of which, like *ced-9(n3377)*, led to viable animals and caused a recessive cell-killing defect and therefore likely maintain the anti-apoptotic but disrupt the pro-apoptotic function of *ced-9*. These alleles—*n6697*, *n6698*, *n6704*, *n6705*, and *n6712*—all contain indels, and in some cases additional missense mutations, in the region encoding the presumptive CED-4–binding pocket and resulted in a cell-killing defect (as assayed by survival of VC-like cells) that was similar in strength to that caused by *ced-9(n3377)* (Fig. 4, A to Q). In addition, we used CRISPR to generate the allele *ced-9(n6730)*, which contains two CED-9 mutations in the presumptive CED-4 binding region, R211E and N212G. CED-9(R211E, N212G) was generated previously by others, expressed in *Escherichia coli*, and shown to be defective in CED-4 binding in vitro (*22*). We found that *ced-9(n6730)* mutants displayed the same phenotype as *n3377*, *n6697*, *n6698*, *n6704*, *n6705*, and *n6712* mutants—viability and a recessive cell-killing defect (Fig. 4, R to T). This observation supports the hypothesis that the phenotype caused by these mutations is a consequence of a disruption in an interaction between CED-9 and CED-4.

These *ced-9* mutations, which are apparently defective in the pro-apoptotic function of *ced-9*, have no apparent effect on the anti-apoptotic function of *ced-9*, as assayed by maternal-effect lethality and ectopic VC cell death (table S2). In short, we identified seven alleles of *ced-9*—as well as one allele of *ced-4*—that prevent the pro-apoptotic function of *ced-9* and disrupt the presumptive CED-9–CED-4 binding region but have no apparent effect on the anti-apoptotic function of *ced-9*. The nature, location, and effects of these mutations suggest that an interaction between CED-9 and CED-4 is required for the pro-apoptotic function of *ced-9* and further suggest that this interaction is not required for the canonical anti-apoptotic function of *ced-9*.

CED-9–CED-4 binding region mutations prevent mitochondrial CED-4 localization in vivo

We next tested if the mutations described above perturb CED-9–dependent sequestration of CED-4 to mitochondria in vivo (*9*). We used a polyclonal antibody against CED-4 previously generated by our laboratory and that in our prior work revealed mitochondrial localization of CED-4 protein in wild-type embryos and perinuclear localization of CED-4 protein in embryos carrying *ced-9(lf)* alleles and a *ced-3* loss-of-function allele (which allowed viability of the strain) (*9*). We confirmed the ability of this antibody to detect CED-4 protein via Western blotting (fig. S1). Using immunofluorescence staining, we also confirmed that wild-type *C. elegans* shows mitochondrial localization of CED-4 (Fig. 5A and fig. S2A) and that embryos carrying the *ced-9* null allele *n2812* and the *ced-3* partial loss-of-function allele *n2427* show perinuclear CED-4 localization (Fig. 5B and fig. S2B). We found that embryos carrying *ced-3(n2427)* and any of the eight CED-9–CED-4 binding region mutant alleles described above—*n3377*, *n6697*, *n6698*, *n6703*, *n6704*, *n6705*, *6712*, and *n6730*—showed perinuclear localization of CED-4 (Fig. 5, C to E, and figs. S2, C to J, and S3, A to E). These observations suggest that these eight mutations, which affect the presumptive CED-9–CED-4 binding regions of CED-4 or CED-9 and cause loss

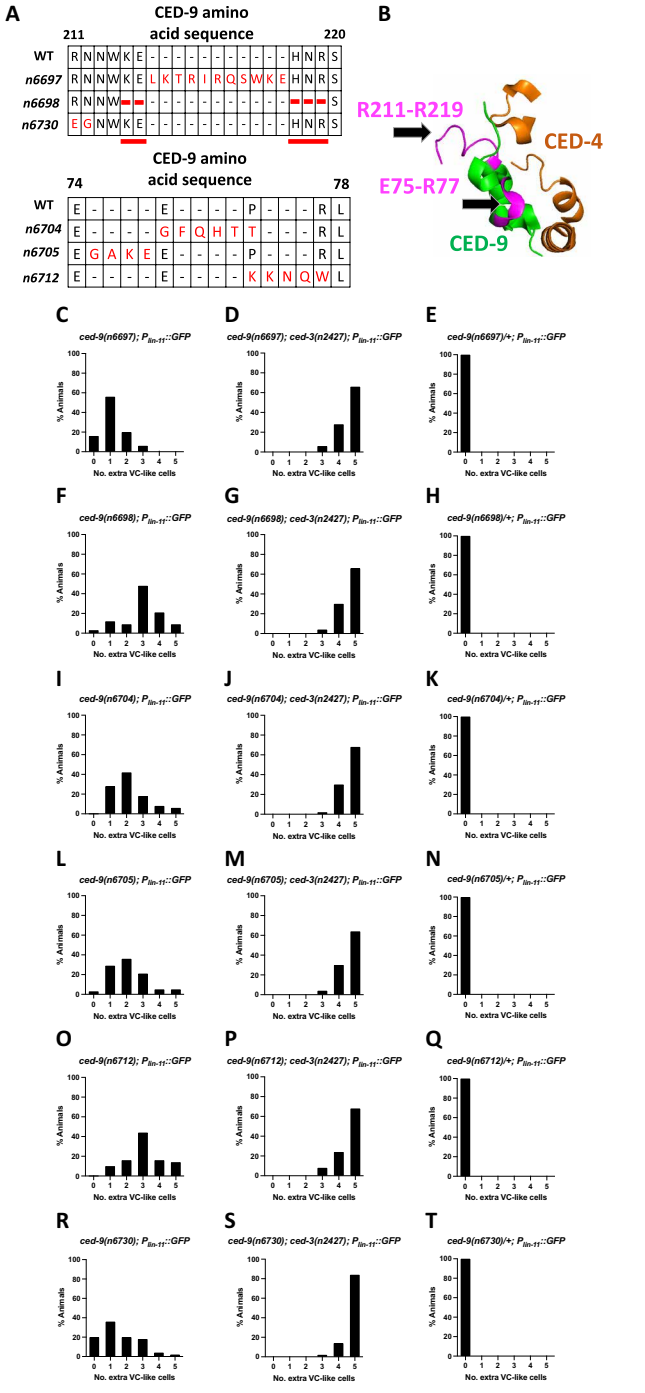

Fig. 4. CRISPR-induced mutations in the CED-9–CED-4 binding region of CED-9 result in cell-killing defects. Six alleles of *ced-9* generated by CRISPR-Cas9 carry mutations likely to disrupt the CED-4 binding region. (**A** and **B**) *ced-9(n6697)* carries an 11 amino acid insertion in the CED-4 binding pocket; *ced-9(n6698)* carries a five amino acid deletion in the CED-4 binding pocket; *ced-9(n6730)* carries two missense mutations, R211E and N212G; *ced-9(n6704)* carries a four amino acid insertion in the CED-4 binding pocket as well as two missense mutations, E75G and P76T; *ced-9(n6705)* carries a four amino acid insertion in the CED-4 binding pocket; and *ced-9(n6712)* carries a three amino acid insertion in the CED-4 binding pocket as well as two missense mutations, P76K and R77W. (**C** to **T**) These mutations are viable in a wild-type background, recessively cause ectopic survival of VC-like cells on their own, and enhance the cell-killing defect caused by *ced-3(n2427)* ($n = 50$).

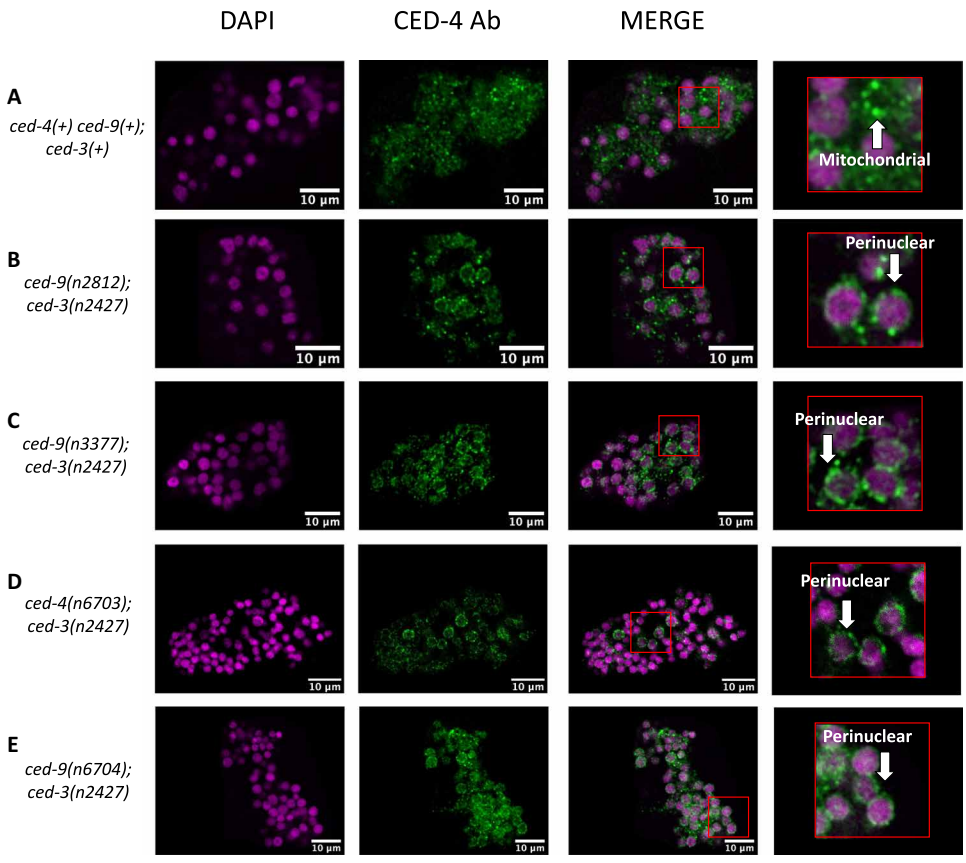

Fig. 5. Mutations that disrupt the CED-9–CED-4 binding regions of either CED-9 or CED-4 result in the mislocalization of CED-4 to the perinuclear membrane. (**A**) Mitochondrial localization of CED-4 in wild-type embryos, as shown previously (*9*) (and fig. S3). (**B**) Perinuclear localization of CED-4 in *ced-9(n2812); ced-3(n2427)* embryos; *ced-9(n2812)* is a null allele of *ced-9*. (**C**) Perinuclear localization of CED-4 in *ced-9(n3377); ced-3(n2427)* embryos. (**D**) Perinuclear localization of CED-4 in *ced-4(n6703); ced-4(n2427)* embryos. (**E**) Perinuclear localization of CED-4 in *ced-9(n6704); ced-3(n2427)* embryos. Images were cropped to avoid background noise, and the brightness and contrast of the DAPI and CED-4 channels were adjusted individually using the Fiji software. Ab, antibody.

of the pro-apoptotic but not anti-apoptotic function of *ced-9*, are defective in a CED-9–CED-4 interaction required to localize CED-4 to mitochondria.

We examined the possibility that the mutant CED-9–CED-4 interaction alleles described above caused translocation of CED-4 to the perinuclear membrane by disrupting the localization of CED-9 rather than by disrupting a CED-9–CED-4 interaction. CED-4(R117S) embryos that expressed endogenously tagged *wrmScarlet::ced-9*(+) showed CED-9(+) localization to mitochondria as expected (fig. S4). We observed a similar mitochondrial localization of CED-9 in CED-4(+) embryos expressing tagged CED-9(+), CED-9(E74K), or CED-9(R211E, N212G) proteins, indicating that the mutant CED-9–CED-4 interaction alleles described above do not disrupt CED-9 localization.

We also tested a CED-9–CED-4 interaction in vitro. In coimmunoprecipitation experiments, the interactions in vitro of CED-9(E74K) with CED-4(+) and those of CED-9(+) with CED-4(R117S) each were reduced compared to the interaction of CED-9(+) with CED-4(+) (fig. S5).

We conclude that mutations that likely disrupt a CED-9–CED-4 physical interaction defined by the crystal structure (*21*) disrupt an in vivo CED-9–CED-4 interaction that localizes CED-4 to mitochondria. We suggest that the loss of this CED-9–CED-4 interaction and possibly the loss of mitochondrial localization of CED-4 are responsible for the loss of the pro-apoptotic function of *ced-9* in these mutants and that neither this CED-9–CED-4 interaction nor CED-9–dependent mitochondrial sequestration of CED-4 is required for the anti-apoptotic function of *ced-9*.

CED-9 binding to CED-4 isoforms is unlikely to explain the pro-apoptotic function of *ced-9*

Because a long isoform of CED-4 can prevent cell death when overexpressed (*23*), it is possible that the mutant CED-9–CED-4 interaction alleles described above disrupt the pro-apoptotic but not the anti-apoptotic function of *ced-9* by interfering with the ability of CED-9 to bind to—and inhibit—the minor anti-apoptotic CED-4L long isoform but not the canonically pro-apoptotic CED-4S short isoform. To assess the endogenous functions of CED-4L and CED-4S, we used CRISPR to mutate the endogenous *ced-4* gene and create alleles of *ced-4* that express only CED-4L [*ced-4(n6692)*] or only CED-4S [*ced-4(n6687)*]. We found that a lack of CED-4S caused a cell-death defect (assayed by ectopic VC cell survival) comparable to that of the *ced-4* null allele *n1162* (fig. S6). By contrast, the absence of CED-4L did not cause any detectable ectopic VC cell death or maternal-effect lethality on its own nor did it suppress the VC cell survival phenotype of *ced-9(n3377)* mutants (fig. S6, D to G). On the basis of these data, we are unable to attribute any endogenous

function to the CED-4L isoform or relate the two CED-4 isoforms to the CED-9–CED-4 interaction alleles we describe above.

DISCUSSION

The pro-apoptotic function of the canonically anti-apoptotic *C. elegans* gene *ced-9* has long been mysterious, suggesting a poorly understood fundamental process at the core of the control of apoptotic cell death. We identified seven alleles of *ced-9* and one allele of *ced-4* that disrupt the pro-apoptotic but not the anti-apoptotic function of *ced-9*. All seven *ced-9* alleles contain mutations in the presumptive CED-4 binding region of CED-9, and the *ced-4* allele contains a mutation in the presumptive CED-9 binding region of CED-4. All eight alleles are thus likely to disrupt an interaction between CED-9 and CED-4. We showed that one of these mutant CED-9 proteins, CED-9(E74K), and the mutant CED-4 protein, CED-4(R117S), disrupted the CED-9–CED-4 interaction in vitro; in similar experiments, another of the mutant CED-9 proteins, CED-9(R211E, N212G), was shown by others to disrupt the CED-9–CED-4 interaction in vitro (*22*). We observed that the seven *ced-9* alleles and the one *ced-4* allele all perturbed the CED-9–CED-4 interaction in vivo, as assayed by perinuclear localization of CED-4 in embryos. None of the seven *ced-9* alleles appeared to cause any detectable defect in the anti-apoptotic function of *ced-9*, despite being highly likely to disrupt the known CED-9–CED-4 interaction. Together, our data support a model in which a CED-9–CED-4 interaction is required for the pro-apoptotic function of *ced-9* but is dispensable for its anti-apoptotic function. Such a model has similarities to that for apoptosis in mammals, in which the anti-apoptotic function of BCL-2 (the mammalian homolog of *ced-9*) does not depend on a direct interaction with APAF-1 (the mammalian homolog of *ced-4*) (*24*, *25*). Despite being apparently unable to bind CED-4 (*26*), human BCL-2 expressed in *C. elegans* reduces cell death (*13*, *27*), consistent with a model in which a CED-9–CED-4 interaction is dispensable for the anti-apoptotic role of CED-9 and suggesting that this anti-apoptotic function is evolutionarily conserved because it can be at least partially performed by BCL-2. Such a model contrasts with the canonical model for caspase-mediated apoptosis in *C. elegans* in which a CED-9–CED-4 protein interaction is required for the anti-apoptotic function of *ced-9*. These findings raise important questions for future inquiry.

First, how does a CED-9–CED-4 interaction promote apoptosis? Possible mechanisms could involve a local binding partner of CED-4, a conformational change or chemical modification of CED-4, or—given the mitochondrial localization of CED-9 and CED-4 in wild-type cells (*9*)—a mitochondrial process that is affected by a CED-9–CED-4 complex. Second, what is the anti-apoptotic function of *ced-9*? The uncoupling of the anti-apoptotic role of *ced-9* from CED-4 mitochondrial localization in CED-9–CED-4 interaction mutants indicates that CED-9 inhibits some process other than CED-4 perinuclear localization. Third, what is the pro-apoptotic event triggered by EGL-1 interaction with CED-9 in cells fated to die if this event is not disruption of the CED-9–CED-4 interaction? Whereas cell death is reduced when a CED-9–CED-4 interaction is perturbed, such a perturbation results in an incomplete block in cell death [e.g., 2.6 extra VC-like cells in *ced-9(n3377); ced-3(+)* animals versus 4.7 extra cells in *ced-9(n3377); ced-3(2427)* animals (Fig. 2, B and C)]; by contrast, an *egl-1* null allele results in a near complete block in cell death (*12*). This difference indicates that EGL-1 interaction with CED-9 promotes cell death by doing more than simply disrupting the presumptive CED-9–CED-4 interaction.

In principle, the answers to these three questions might all involve a single unknown mechanism. Two nonmutually exclusive possibilities consistent with our data are as follows:

1) The binding of EGL-1 to the CED-9–CED-4 complex triggers a pro-apoptotic process (Fig. 6A). Loss of a CED-9–CED-4 interaction prevents this EGL-1–CED-9–CED-4 interaction and the pro-apoptotic process that it promotes.

2) The anti-apoptotic function of *ced-9* is to block a pro-apoptotic process dependent on CED-4 and CED-3 but independent of CED-4 sequestration to mitochondria by CED-9 (Fig. 6B).

A more specific model that incorporates both of these concepts is depicted in Fig. 6 (D to G): EGL-1 interaction with CED-9 activates

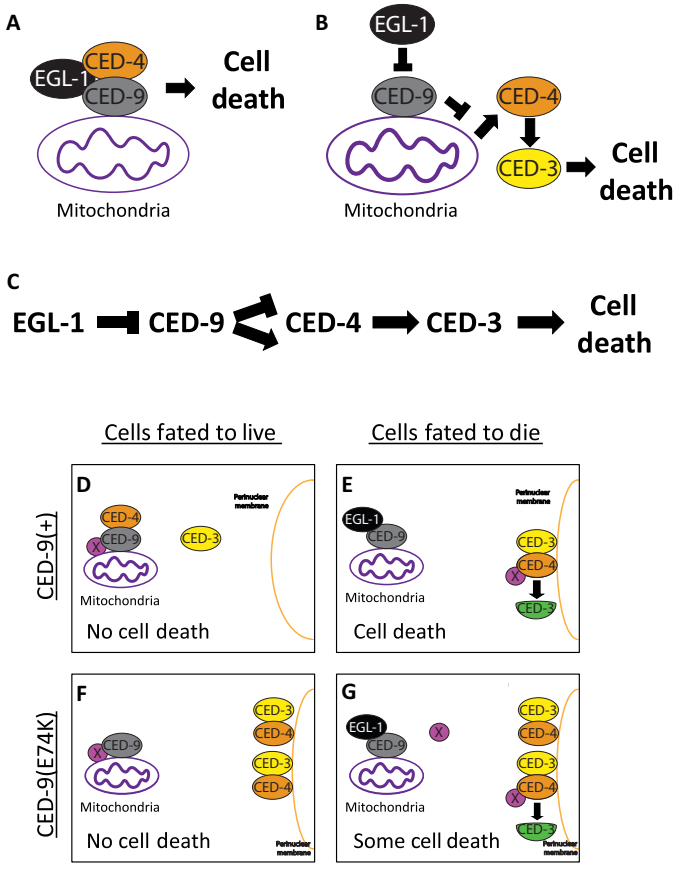

Fig. 6. Possible alternatives to the canonical apoptosis pathway. (**A**) EGL-1 binding to the CED-9–CED-4 complex promotes a pro-apoptotic process dependent on a CED-9–CED-4 interaction. (**B**) EGL-1 blocks the ability of CED-9 to prevent a pro-apoptotic process occurring independently of CED-4 sequestration by CED-9. (**C**) Alternative genetic pathway in which CED-9 has both an anti-apoptotic and pro-apoptotic function that depend on CED-4 and CED-3. (**D** to **G**) An unknown (essential or genetically redundant) factor X promotes apoptosis through CED-4 activation. (D) In CED-9(+) cells fated to live, both factor X and CED-4 are sequestered to mitochondria by CED-9. (E) In CED-9(+) cells fated to die, EGL-1 changes the conformation of CED-9, releasing factor X–activated CED-4, which then translocates to the perinuclear membrane and initiates cell death. (F) CED-9–CED-4 binding mutants, such as *ced-9(n3377)* [E74K], maintain CED-9–dependent factor X sequestration, preventing killing in cells fated to live. (G) In cells fated to die carrying CED-9–CED-4 binding mutations, EGL-1 releases factor X from CED-9; CED-4 and factor X do not interact at mitochondria, leading to inefficient CED-4 activation by factor X and resulting in only some cell death.

a cell-death promoting factor or process (labeled "X") that activates CED-4. CED-4 activation by X occurs more efficiently at mitochondria but can still occur, albeit less effectively, when CED-4 is not at mitochondria (such as in CED-9–CED-4 interaction mutants). X could reflect a pro-apoptotic factor from mitochondria that interacts with CED-4, a CED-4 conformational change, a chemical modification of CED-4, or CED-4 oligomerization. A model in which CED-9 sequesters a pro-apoptotic factor that activates CED-4 upon its release from mitochondria closely mirrors the mechanism of APAF-1 activation by mammalian BCL-2 family members via the release of cytochrome c from mitochondria (*28*–*32*).

It is also possible that CED-9 and CED-4 have two distinct physical interactions: one that is anti-apoptotic and one that is pro-apoptotic. In such a model, CED-4(R117S) and the CED-9 mutations that result in ectopic cell survival and viability disrupt the pro-apoptotic but not the anti-apoptotic interaction. In this model, the anti-apoptotic role of CED-9 is as in the canonical model and dependent on a CED-9–CED-4 interaction distinct from that defined by crystal structure studies to date (*21*), while the pro-apoptotic role of CED-9 depends on the CED-4 interaction defined by the crystal structure (*21*), which is distinct from the canonical, anti-apoptotic interaction. We tested one plausible model involving two distinct physical interactions in which the CED-9–CED-4 interaction mutants described above specifically perturb the CED-9 interaction with either the major and pro-apoptotic CED-4S or the minor and apparently anti-apoptotic CED-4L isoform of CED-4. However, we failed to identify any endogenous function for CED-4L, and the phenotype of animals retaining CED-4L and lacking CED-4S and that of animals lacking *ced-4* function altogether were no different (fig. S6). These data do not support a model in which the CED-9–CED-4 interaction mutants we describe differentially affect interactions of CED-9 with the two CED-4 isoforms.

In short, we report that an interaction between the BCL-2 homolog CED-9 and its pro-apoptotic binding partner the APAF-1 homolog CED-4 promotes apoptosis in *C. elegans*, the animal in which caspase-driven apoptosis was found. Like CED-9, the mammalian protein BCL-2 and other anti-apoptotic BCL-2 family members can be pro-apoptotic, as is the case for BCL-2 in the presence of the nuclear hormone receptor NUR77 (*33*). Despite extensive research spanning decades, the pro-apoptotic mechanism(s) of these bifunctional proteins remains poorly understood. One difficulty in elucidating such mechanisms might be the complexity of mammalian apoptosis pathways, a consequence in part of the relatively large number of BCL-2 family members in mammals. By contrast, CED-9 is the only BCL-2 family member in *C. elegans*. In addition, by using *C. elegans*, the functions of and interactions among cell-death proteins expressed at endogenous levels can be easily analyzed in the intact organism, features more difficult to attain using mammals or mammalian cell culture in vitro systems.

The pro-apoptotic function of *ced-9* is lost when a CED-9–CED-4 interaction is disrupted and CED-4 translocates away from mitochondria, suggesting that mitochondrial localization is important in promoting CED-4 activation and consequent apoptosis in *C. elegans*. In mammals, pro-apoptotic members of the BCL-2 family, such as BAX and BAK, promote apoptosis by forming pores in and permeabilizing the mitochondrial outer membrane and thereby releasing cytochrome c, which activates APAF-1, the mammalian homolog of *C. elegans* CED-4. *C. elegans* lacks such pore-forming pro-apoptotic BCL-2 family members, raising the question of why CED-4 activation might involve mitochondrial localization. Given the notable conservation of cell-death proteins and pathways between *C. elegans* and mammals and the apparently conserved role of mitochondria in CED-9/BCL-2–dependent CED-4/APAF-1 activation, the answer to this question might add a key insight concerning the fundamental process of apoptosis and suggest novel targets for therapeutics aimed at treating disorders that involve dysregulated apoptosis, such as certain neurodegenerative disorders and cancers.

MATERIALS AND METHODS

C. elegans strain maintenance

All strains were cultured on nematode growth medium (NGM) plates seeded with the *E. coli* strain OP50 at 20°C as described previously (*34*) unless otherwise indicated.

Immunostaining

Embryos were collected by dissolving adult worms in bleach solution (0.5 M NaOH/0.8% sodium hypochlorite) for ~10 min (*35*). Embryos were then fixed and permeabilized essentially as described previously (*36*). Previously described rat antiserum against CED-4 was used for this study (*9*). We purified the rat antiserum against CED-4 using a Melon Gel IgG Purification Kit from Thermo Fisher Scientific (catalog no. 45206). Purified anti–CED-4 antibody was diluted to 10 μg/ml for immunofluorescence staining and then stained with a secondary antibody, goat anti-Rat IgG (H+L) Cross-Adsorbed Secondary Antibody, Alexa Fluor 647 from Thermo Fisher Scientific (catalog no. A-21247, RRID:AB_141778). Embryos were then mounted using a SlowFade Diamond Antifade Mountant with 4′,6-diamidino-2-phenylindole (DAPI) from Thermo Fisher Scientific (catalog no. S36964). Images of anti–CED-4 stained embryos were obtained using a 63x objective on an LSM 800 confocal microscope from Zeiss, Oberkochen, Germany (Zeiss LSM 800 with Airyscan Microscope, RRID:SCR_015963) and ZEN software. Images were obtained via confocal microscopy and, due to variability in the intensity of signal associated with in vivo immunofluorescence staining due to the freeze-cracking protocol used, channels (DAPI, MitoFluor, and CED-4) were processed individually using the Fiji software (Fiji, RRID:SCR_002285) (*37*). For examining mitochondria localization in antibody staining experiments, MitoFluor Red 589 from Thermo Fisher Scientific (catalog no. M-22424) was fed to adult worms at a concentration of 10 μg/ml by covering the lawn of OP50 and incubating overnight at 20°C essentially as described previously (*38*). Images were then cropped to reduce background. For examining mitochondrial localization in embryos carrying *wrmScarlet::ced-9*, MitoTracker Deep Red FM (Thermo Fisher Scientific, catalog no. M22426) was reconstituted in dimethyl sulfoxide (DMSO) (MilliporeSigma, product no. D8418) at a stock concentration of 1 mM. Twenty L4 worms were incubated overnight in the dark at 20°C on NGM petri plates seeded with *E. coli* OP50 containing either 5 μM MitoTracker Deep Red FM or 200X dilution of DMSO. Embryos were washed off the plates with M9 and imaged using confocal microscopy (Zeiss LSM 800 with Airyscan Microscope, RRID:SCR_015963) and ZEN software. Images were processed using the Fiji software (Fiji, RRID:SCR_002285) (*37*). Cartoon images were created using Adobe Illustrator (Adobe Illustrator, RRID:SCR_010279) and Microsoft PowerPoint.

VC-like cell counts

The number of VC-like cells was assessed by counting the number of cells expressing the transgene *nIs106* in L4-stage worms ($n = 50$

for each genotype) using a Nikon SMZ18 fluorescent dissecting microscope (*20*). Counts were visualized using GraphPad Prism (RRID:SCR_002798).

CRISPR-induced mutations

CRISPR mutants were generated by injecting early adult-stage worms carrying the transgene *nIs106* with Cas9 protein with a guide RNA (gRNA) targeting the gene *dpy-10* as well as a *dpy-10* repair template DNA and *ced-9* or *ced-4* repair template DNA (varying with each round of injection based on the gRNA) as described previously (*39*). *ced-9* mutations in the CED-4 binding pocket were generated by using target gRNAs against various locations in the CED-4 binding pocket based on the CED-9–CED-4 crystal structure (*21*); viable progeny showing extra VC-like cells were then picked and propagated. Structural images of the CED-9–CED-4 complex were generated based on the CED-9–CED-4 crystal structure using PyMOL (*21*, *40*). To create a *wrmScarlet*::*ced-9* knock-in strain, a polymerase chain reaction product containing sequences for *wrmScarlet* and a flexible linker 3x(Gly-Gly-Ser-Gly) was inserted just upstream of the start codon of *ced-9*. The DNA melting method was applied to prepare the repair template, as described previously (*41*).

His-mediated pulldown assay

Truncated CED-9, CED-9[1-251], and full-length CED-4S protein were cloned as glutathione *S*-transferase (GST) fusion proteins into the vector pGEX-2T and as a 6x-His fusion protein into the vector pET-28b, respectively. CED-9 and CED-4 fusion proteins were overexpressed in the *E. coli* strain BL21(DE3) essentially as described previously (*22*). Competent cells were obtained from Thermo Fisher Scientific (catalog no. EC0114). *E. coli* strains coexpressing both plasmids were then pelleted, and pellets were resuspended in 5 ml of a lysis buffer [25 mM Tris (pH 8.0), 300 mM NaCl, 2 mM dithiothreitol (DTT), DNase I, and a Thermo Fisher Scientific Pierce Protease Inhibitor Tablet (catalog no. A32963)] and sonicated. The CED-4 protein was detected in these samples by Western blot using a Thermo Fisher Scientific 6x-His tag monoclonal antibody (catalog no. MA1-21315). The relative amount of CED-4 protein was determined using the Fiji software (Fiji, RRID:SCR_002285) (*37*), and 1 ml of the cell lysate normalized to the relative amount of CED-4 protein present was then allowed to bind with 60 μl of the Thermo Fisher Scientific HisPur Ni-NTA slurry (catalog no. 88221), which was washed twice with 500 μl of a wash buffer [25 mM Tris (pH 8.0), 300 mM NaCl, 2 mM DTT, and 25 mM imidazole (from 1 M stock at pH 8.0)] (*21*). The protein was allowed to incubate with the slurry at 4°C for 2 hours with rotation. The resin was then washed four times with 500 μl of the wash buffer and eluted with 45 μl of the Bio-Rad 4x Laemmli Sample Buffer (catalog no. 1610747) with DTT. Ten microliters of the sample was then resolved by SDS–polyacrylamide gel electrophoresis (PAGE) on a Bio-Rad (Hercules, CA) 10% Mini-PROTEAN TGX Precast Protein Gel (catalog no. 456-1034) and transferred to a Bio-Rad 0.45-μm nitrocellulose membrane (catalog no. 1620115) using a Thermo Fisher Scientific Pierce G2 Fast Blotter (catalog no. 62289). The CED-4 protein was visualized using a 1/2000 dilution of a Thermo Fisher Scientific 6x-His tag monoclonal antibody (catalog no. MA1-21315) and a 1/10,000 dilution of a Thermo Fisher Scientific Goat anti-Mouse IgG (H+L) Highly Cross-Adsorbed Secondary Antibody, Alexa Fluor Plus 647 (catalog no. A32728). The CED-9 protein was visualized using a 1/3000 dilution of a Thermo Fisher Scientific GST tag polyclonal antibody (catalog no. A5800) and a 1/10,000 dilution of Goat anti-Rabbit IgG (H+L) Highly Cross-Adsorbed Secondary Antibody, Alexa Fluor Plus 488 (catalog no. A32731).

Western blot analysis

Protein was extracted from mixed-stage *C. elegans* embryos via 10 min of sonication at 80°C and 2 min of boiling at 95°C essentially as described previously (*42*). One hundred micrograms of the protein extracted from mixed-staged embryos was then resolved by SDS-PAGE on a Bio-Rad (Hercules, CA) 10% Mini-PROTEAN TGX Precast Protein Gel (catalog no. 456-1034) and transferred to a Bio-Rad 0.45-μm nitrocellulose membrane (catalog no. 1620115) using a Thermo Fisher Scientific Pierce G2 Fast Blotter (catalog no. 62289). The CED-4 protein was detected using the previously described purified rat anti–CED-4 antibody at a concentration of 12 μg/ml, and the secondary antibody, goat anti-Rat IgG (H+L) Cross-Adsorbed Secondary Antibody, Alexa Fluor 647 from Thermo Fisher Scientific, (catalog no. A-21247, RRID:AB_141778) was used at a concentration of 2 μg/ml essentially as described previously (*42*). Protein band size was determined using Bio-Rad Precision Plus Protein Dual Color Standards (catalog no. 1610374).

Supplementary Materials

This PDF file includes:

Tables S1 to S4
Figs. S1 to S6

REFERENCES AND NOTES

1. M. D. Jacobson, M. Weil, M. C. Raff, Programmed cell death in animal development. *Cell* **88**, 347–354 (1997).
2. Y. Fuchs, H. Steller, Programmed cell death in animal development and disease. *Cell* **147**, 742–758 (2011).
3. D. R. Hipfner, S. M. Cohen, Connecting proliferation and apoptosis in development and disease. *Nat. Rev. Mol. Cell Biol.* **5**, 805–815 (2004).
4. O. Takeuchi, J. Fisher, H. Suh, H. Harada, B. A. Malynn, S. J. Korsmeyer, Essential role of BAX, BAK in B cell homeostasis and prevention of autoimmune disease. *Proc. Natl. Acad. Sci. U.S.A.* **102**, 11272–11277 (2005).
5. B. T. Hyman, J. Yuan, Apoptotic and non-apoptotic roles of caspases in neuronal physiology and pathophysiology. *Nat. Rev. Neurosci.* **13**, 395–406 (2012).
6. H. M. Ellis, H. R. Horvitz, Genetic control of programmed cell death in the nematode *C. elegans*. *Cell* **44**, 817–829 (1986).
7. M. O. Hengartner, R. E. Ellis, H. R. Horvitz, *Caenorhabditis elegans* gene *ced-9* protects cells from programmed cell death. *Nature* **356**, 494–499 (1992).
8. G. Lettre, M. O. Hengartner, Developmental apoptosis in *C. elegans*: A complex CEDnario. *Nat. Rev. Mol. Cell Biol.* **7**, 97–108 (2006).
9. F. Chen, B. M. Hersh, B. Conradt, Z. Zhou, D. Riemer, Y. Gruenbaum, H. R. Horvitz, Translocation of *C. elegans* CED-4 to nuclear membranes during programmed cell death. *Science* **287**, 1485–1489 (2000).
10. A. M. Chinnaiyan, K. O'Rourke, B. R. Lane, V. M. Dixit, Interaction of CED-4 with CED-3 and CED-9: A molecular framework for cell death. *Science* **275**, 1122–1126 (1997).
11. M. S. Spector, S. Desnoyers, D. J. Hoeppner, M. O. Hengartner, Interaction between the *C. elegans* cell-death regulators CED-9 and CED-4. *Nature* **385**, 653–656 (1997).
12. B. Conradt, H. R. Horvitz, The *C. elegans* protein EGL-1 is required for programmed cell death and interacts with the Bcl-2–like protein CED-9. *Cell* **93**, 519–529 (1998).
13. M. Hengartner, H. R. Horvitz, *C. elegans* cell survival gene *ced-9* encodes a functional homolog of the mammalian proto-oncogene *bcl-2*. *Cell* **76**, 665–676 (1994).
14. E. Pourkarimi, S. Greiss, A. Gartner, Evidence that CED-9/Bcl2 and CED-4/Apaf-1 localization is not consistent with the current model for *C. elegans* apoptosis induction. *Cell Death Differ.* **19**, 406–415 (2012).
15. H. Duan, A. M. Chinnaiyan, P. L. Hudson, J. P. Wing, W.-W. He, V. M. Dixit, ICE-LAP3, a novel mammalian homologue of the *Caenorhabditis elegans* cell death protein CED-3 is activated during Fas- and tumor necrosis factor-induced apoptosis. *J. Biol. Chem.* **271**, 1621–1625 (1996).

16. F. Cecconi, G. Alvarez-Bolado, B. I. Meyer, K. A. Roth, P. Gruss, Apaf1 (CED-4 homolog) regulates programmed cell death in mammalian development. *Cell* **94**, 727–737 (1998).
17. R. Nehme, B. Conradt, *egl-1*: A key activator of apoptotic cell death in *C. elegans*. *Oncogene* **27**, S30–S40 (2008).
18. J. E. Sulston, H. R. Horvitz, Post-embryonic cell lineages of the nematode, *Caenorhabditis elegans*. *Dev. Biol.* **56**, 110–156 (1977).
19. J. G. White, E. Southgate, J. N. Thomson, S. Brenner, The structure of the nervous system of the nematode *Caenorhabditis elegans*. *Philos. Trans. R. Soc. Lond. B Biol. Sci.* **314**, 1–340 (1986).
20. P. W. Reddien, E. C. Andersen, M. C. Huang, H. R. Horvitz, DPL-1 DP, LIN-35 Rb and EFL-1 E2F act with the MCD-1 zinc-finger protein to promote programmed cell death in *Caenorhabditis elegans*. *Genetics* **175**, 1719–1733 (2007).
21. N. Yan, J. Chai, E. S. Lee, L. Gu, Q. Liu, J. He, J.-W. Wu, D. Kokel, H. Li, Q. Hao, D. Xue, Y. Shi, Structure of the CED-4–CED-9 complex provides insights into programmed cell death in *Caenorhabditis elegans*. *Nature* **437**, 831–837 (2005).
22. N. Yan, L. Gu, D. Kokel, J. Chai, W. Li, A. Han, L. Chen, D. Xue, Y. Shi, Structural, biochemical, and functional analyses of CED-9 recognition by the proapoptotic proteins EGL-1 and CED-4. *Mol. Cell* **15**, 999–1006 (2004).
23. S. Shaham, H. R. Horvitz, An alternatively spliced *C. elegans ced-4* RNA encodes a novel cell death inhibitor. *Cell* **86**, 201–208 (1996).
24. K. Moriishi, D. C. S. Huang, S. Cory, J. M. Adams, Bcl-2 family members do not inhibit apoptosis by binding the caspase activator Apaf-1. *Proc. Natl. Acad. Sci. U.S.A.* **96**, 9683–9688 (1999).
25. S. Conus, T. Rossé, C. Borner, Failure of Bcl-2 family members to interact with Apaf-1 in normal and apoptotic cells. *Cell Death Differ.* **7**, 947–954 (2000).
26. A. M. Jabbour, M. A. Puryer, J. Y. Yu, T. Lithgow, C. D. Riffkin, D. M. Ashley, D. L. Vaux, P. G. Ekert, C. J. Hawkins, Human Bcl-2 cannot directly inhibit the *Caenorhabditis elegans* Apaf-1 homologue CED-4, but can interact with EGL-1. *J. Cell Sci.* **119**, 2572–2582 (2006).
27. D. L. Vaux, I. L. Weissman, S. K. Kim, Prevention of programmed cell death in *Caenorhabditis elegans* by human *bcl-2*. *Science* **258**, 1955–1957 (1992).
28. X. Liu, C. N. Kim, J. Yang, R. Jemmerson, X. Wang, Induction of apoptotic program in cell-free extracts: Requirement for dATP and cytochrome c. *Cell* **86**, 147–157 (1996).
29. R. M. Kluck, E. Bossy-Wetzel, D. R. Green, D. D. Newmeyer, The release of cytochrome c from mitochondria: A primary site for Bcl-2 regulation of apoptosis. *Science* **275**, 1132–1136 (1997).
30. J. Yang, X. Liu, K. Bhalla, C. N. Kim, A. M. Ibrado, J. Cai, T.-I. Peng, D. P. Jones, X. Wang, Prevention of apoptosis by Bcl-2: Release of cytochrome c from mitochondria blocked. *Science* **275**, 1129–1132 (1997).
31. H. Zou, W. J. Henzel, X. Liu, A. Lutschg, X. Wang, Apaf-1, a human protein homologous to *C. elegans* CED-4, participates in cytochrome c-dependent activation of caspase-3. *Cell* **90**, 405–413 (1997).
32. P. Li, D. Nijhawan, I. Budihardjo, S. M. Srinivasula, M. Ahmad, E. S. Alnemri, X. Wang, Cytochrome c and dATP-dependent formation of Apaf-1/caspase-9 complex initiates an apoptotic protease cascade. *Cell* **91**, 479–489 (1997).
33. B. Lin, S. K. Kolluri, F. Lin, W. Liu, Y. H. Han, X. Cao, M. I. Dawson, J. C. Reed, X. K. Zhang, Conversion of Bcl-2 from protector to killer by interaction with nuclear orphan receptor Nur77/TR3. *Cell* **116**, 527–540 (2004).
34. S. Brenner, The genetics of *Caenorhabditis elegans*. *Genetics* **77**, 71–94 (1974).
35. C. Guenther, G. Garriga, Asymmetric distribution of the *C. elegans* HAM-1 protein in neuroblasts enables daughter cells to adopt distinct fates. *Development* **122**, 3509–3518 (1996).
36. D. Korčeková, A. Gombitová, I. Raška, D. Cmarko, C. Lanctôt, Nucleologenesis in the *Caenorhabditis elegans* embryo. *PLOS ONE* **7**, e40290 (2012).
37. J. Schindelin, I. Arganda-Carreras, E. Frise, V. Kaynig, M. Longair, T. Pietzsch, S. Preibisch, C. Rueden, S. Saalfeld, B. Schmid, J.-Y. Tinevez, D. J. White, V. Hartenstein, K. Eliceiri, P. Tomancak, A. Cardona, Fiji: An open-source platform for biological-image analysis. *Nat. Methods* **9**, 676–682 (2012).
38. S. Dingley, E. Polyak, R. Lightfoot, J. Ostrovsky, M. Rao, T. Greco, H. Ischiropoulos, M. J. Falk, Mitochondrial respiratory chain dysfunction variably increases oxidant stress in *Caenorhabditis elegans*. *Mitochondrion* **10**, 125–136 (2010).
39. D. J. Dickinson, B. Goldstein, CRISPR-based methods for *Caenorhabditis elegans* genome engineering. *Genetics* **202**, 885–901 (2016).
40. Schrödinger LLC, The PyMOL Molecular Graphics System, Version 1.8 (Schrödinger, 2015).
41. K. S. Ghanta, C. C. Mello, Melting dsDNA donor molecules greatly improves precision genome editing in *Caenorhabditis elegans*. *Genetics* **216**, 643–650 (2020).
42. D.-E. Jeong, Y. Lee, S.-J. V. Lee, Western blot analysis of *C. elegans* proteins. *Methods Mol. Biol.* **1742**, 213–225 (2018).

Acknowledgments: We thank J. Kong, I. Kesisova, C. Diehl, and other members of the Horvitz laboratory for discussions. H.R.H. is the David H. Koch Professor of Biology at MIT and an investigator of the Howard Hughes Medical Institute. **Funding:** N.T. was supported by a Ludwig Center Graduate Student Fellowship and NIH grant T32 GM007287. M.H.X.L. was supported by NSF grant DGE 2140743. This work was supported by NIH grant R01 GM024663.
Author contributions: Conceptualization: N.T., P.R., and H.R.H. Methodology: N.T., P.R., B.H., and H.R.H. Investigation: N.T., P.R., B.H., D.L., and M.H.X.L. Writing—original draft: N.T. and H.R.H. Funding acquisition: N.T. and H.R.H. Resources: N.T., B.H., and H.R.H. Supervision: H.R.H.
Competing interests: The authors declare that they have no competing interests. **Data and materials availability:** All data needed to evaluate the conclusions in the paper are present in the paper and/or the Supplementary Materials.

Submitted 21 November 2023
Accepted 4 September 2024
Published 9 October 2024
10.1126/sciadv.adn0325